Using the Ultra-relativistic Quantum Molecular Dynamics (UrQMD) model to extract the thermal conductivity transport coefficient of hadron gas.

Thendo Emmanuel Nemakhavhani (200824451).

A dissertation submitted to the Faculty of Science,

University of Johannesburg, South Africa,

in fulfillment of the requirments for the

Degree of Magister Science (M.Sc.) in Physics.

Johannesburg, 2016

Candidate's Declaration

I, the undersigned, hereby declare that the work contained in this dissertation is my original work, and that any work done by others or by myself previously has been acknowledged and referenced accordingly.

Thendo Emmanuel Nemakhavhani

_____ day of _____ 2016

Abstract

Thermal conductivity of hadron matter is studied using a microscopic transport model, which can support the newly Large Hadron Collider (LHC) energy of up to $\sqrt{s} = 14$ TeV, namely the Ultra-relativistic Quantum Molecular Dynamics (UrQMD). The molecular dynamics simulation is performed for a system of light mesons species (π, ρ, K) in a box with periodic boundary conditions. Equilibrium state is investigated by studying chemical equilibrium and thermal equilibrium of the system. Particle multiplicity equilibrates with time, and the energy spectra of different light mesons species have the same slopes and common temperatures when thermal equilibrium is reached. Thermal conductivity transport coefficient is calculated from the heat current - current correlations using the Green-Kubo relations.

Acknowledgments

I would like to thank Professor A. Muronga and Miss L. T. Stewart for helping me with this thesis in terms of corrections and discussions. Mr Snymann Andrea who helped me with computational software's needed for this studies. Financial support from NIThep is acknowledged.

Contents

Chapter 1

Introduction

A large number of studies in heavy ion physics and high energy physics have been done using the results produced from Relativistic Heavy Ion Collider (RHIC). Now with the restart of the Large Hadron Collider (LHC) physics programme, the field of high energy nuclear physics, and especially heavy ion physics, has gone into a new era. It is now possible to explore the properties of Quantum-Chromo-Dynamics (QCD) at unprecedented particle densities and temperatures at much higher energy than that produced at RHIC from $\sqrt{s} = 200$ GeV to $\sqrt{s} = 14$ TeV at LHC [1, 2].

High energy heavy ion reactions are studied experimentally and theoretically to obtain information about the properties of nuclear matter under extreme conditions at high densities and temperature as well as about the phase transition to new state of matter, quark-gluon plasma (QGP) [3, 4, 5]. The ultimate goal of a theoretical description of heavy ion collisions is a derivation and solution of equations of motion for the elementary degrees of freedom, the quarks, gluons and hadrons thus knowledge of transport equation of nuclear collisions and

that of kinetic theory is of importance [6]. This work reports on the transport coefficient namely, thermal conductivity of hadron matter. Other transport coefficients such as shear and bulk viscosity are well discussed and documented [5, 7], but the study of thermal conductivity transport coefficient is poorly documented especially with the use of UrQMD model to simulate ultra-relativistic heavy ion collisions. To study the transport coefficient of hadronic matter, we must consider an equilibrated system, hence we study the equilibration of this system in infinite hadronic matter using microscopic transport model the UrQMD which can now support new LHC energy of $\sqrt{s} = 2.76$ TeV for Pb+Pb central collisions [3, 6, 8, 9, 10].

The Ultra-relativistic Quantum Molecular Dynamics model is a microscopic model used to simulate ultra-relativistic heavy ion collisions in the energy range from Bevalac and SIS up to Alternating Gradient Synchrotron (AGS), The Super Proton Synchrotron (SPS), RHIC and now the LHC. The main goals are to gain the understanding about the following physical phenomena within a single transport model which are the creation of dense hadronic matter at high temperatures, properties of nuclear matter, Delta and Resonance matter, creation of mesonic matter and of anti-matter, creation and transport of rare particles in hadronic matter, modification and destruction of strangeness in matter and emission of electromagnetic probes.

UrQMD is a microscopic transport approach based on the covariant propagation of constituent (anti)quarks and diquarks accompanied by mesons and baryons, as well as the corresponding antiparticles, i.e. full baryon, antibaryon symmetry are included [11]. The UrQMD is a dubbed model and such a microscopic model is based on a phase space description of the reaction and that can

incorporate different reaction mechanisms which are able to yield observables [6].

Equilibration of the system is studied by evaluating particle number densities from chemical equilibrium, energy spectra as well as the temperatures from thermal equilibrium of different light meson species in a cubic box with periodic boundary conditions. This means that if a particle leaves the box another particle with the same momentum enters the box from other side [12, 13]. Equilibration times depend critically on energy and baryon densities. Energy spectra of various hadronic species are shown to be isotropic and consistent with a single temperature in equilibrium [14].

This study is restricted to a system that only contains meson resonance as a degree of freedom. The infinite hadron matter which is composed of particles made out of quarks held together by strong force and can be categorized in two forms which are baryons (made of 3 quarks) and mesons (made of up and down quarks) is modelled by initializing the system by light mesons species namely the pion (π), the rho (ρ) and the kaon (K) [5]. Only light meson are considered for this study as they are easy to work with because of their low mass especially for a new study whereby not much work has been done and documented on. For this study a cubic box with volume V and fixed baryon number density is considered.

We also pay attention to the Equation of State (EoS) of hot and dense hadron gas as it is an important quantity in high energy nuclear physics. The knowledge of the EoS is important for better understanding of the final state of interactions which is dominated by hadrons produced during ultra-relativistic heavy ion collisions. Transport coefficients and EoS for hadron gas are a major

source of uncertainties in dissipative fluid dynamics [5, 10]. Transport coeffcients provide the response of the system to thermodynamic forces that take it out of equilibrium [15].

The equation of State of nuclear matter is one of the key points to gain further understanding since the EoS directly provides the relationship between pressure and energy at a given net-baryon density [11].

1.1 Thermal conductivity transport coefficient

In simplified terms, thermal conductivity is the ability of material (in our case it would be the hadron gas) to conduct heat. This study focuses on the thermal conductivity of hadron gas which in heavy ion physics and high energy physics is known as thermal conductivity transport coefficient.

Thermal conductivity has been largely neglected and one of the reason for neglegence is that thermal conductivity in most fluid-dynamical calculations in the field attempt to describe the QGP only at midrapidity and very high energies, where baryon number and its corresponding chemical potential are approximately zero [16]. In a system where QGP is described at smaller collision energies, such as the ones probed in RHIC, baryon number can no longer be ignored and thermal conductivity might play a more decisive role [16].

A better understanding and more details are required for thermal conductivity transport coefficient as this coefficient is important in the improvement of high energy heavy ion collision experiments like LHC and model such as the UrQMD model.

To study thermal conductivity transport coefficient for hadron gas, a microscopic model that includes realistic interactions among hadrons is used. Thus

one adopts a relativistic microscopic model, the UrQMD and perform molecular dynamical simulations for hadron gas of meson [5].

We focus on the hadronic scale temperature (100 MeV $< T <$ 200 MeV) and zero baryon number density which is expected to be realized in the central high energy nuclear collisions [8]. We change energy density from ε = 0.1 - 0.5 GeV/fm^3 and for each energy density we run the system with 200 events while keeping volume and baryon number density constant until the equilibrium state is reached. Thermal conductivity transport coefficient is calculated from the heat current - current correlations using the Green-Kubo relations.

The Green-Kubo relations gives the mathematical expression for transport coefficients in terms of integrals over time of heat flux correlation functions [17]. Green and Kubo showed that transport coefficients like conductivity, shear and bulk viscosity can be related to the correlation functions of the corresponding flux or tensor in thermal equilibrium [18, 19].

1.2 Short description of pion, rho and kaon mesons

1.2.1 Pion

In particle physics a pion is a short description of pi-meson and it is denoted by the symbol π. It consist of three subatomic particles which are π^0, π^+, and π^-. Each pion consists of quark and antiquark and is therefore called a meson. The pions are also known as the lightest particles in their meson group and plays an important role in explaining the low-energy properties of strong nuclear force.

It is considered unstable having a positive and negative charge decaying with mean life time of about 26×10^{-9} seconds with pi-zero decaying at even shorter life time [20].

1.2.2 Kaon

Just like pion, kaon is known as K-meson and denoted by the letter K. The kaon are understood to be bound state of strange quark or antiquark and up and down quark or antiquark. The kaon consists of three subatomic particles K^0, K^+ and K^- and falls under Bosonic statistics. The kaon decays into three pions $2\pi^+$, and $1\pi^-$ due to the process that involves both the weak and the strong interactions [20].

1.2.3 Rho

In particle physics, a rho-meson which is denoted by symbol ρ is a short-lived hadronic particle that is an isospin triplet whose three states are denoted as ρ^+, ρ^0 and ρ^-. The rho mesons can be interpreted as a bound state of a quark and an anti-quark and is an excited version of the pion.

After pions and kaons, rho mesons are the lightest strongly interacting particles with a mass of roughly 770 MeV for all three states. The rho mesons have a very short lifetime and their decay width is about 145 MeV with the peculiar feature that the decay widths are not described by a Breit-Wigner [21] form. The principal decay route of the rho mesons is to a pair of pions with a branching rate of 99.9 [20].

1.3 Description outline

The rest of the thesis is organized as follows: In chapter 2. Introduction to relativistic kinetic theory: While studying transport coefficients of hadronic matter, knowledge of relativistic kinetic theory is required so that one would be able to understand and define basic physics terms, formulae and tensor notation used. It is of importance to understand terms such as four-vector, hydrodynamic 4-velocity, metric tensor, energy momentum tensor and particle four flow to name a few. This chapter is important as most of the notations, definitions and equations mentioned here will be used throughout the study.

In chapter 3. Short description of the UrQMD model: The UrQMD model is the important tool for this study as it will be used to simulate ultra-relativistic heavy ion collisions similar to those produced at LHC and RHIC. The model will be discussed and how it is initialized for different simulations according to the preference of the individual. The different mesons and baryons species included in the model are also discussed. The input file to simulate different collisions and the output file where the collisions history is written on will be discussed in this also.

In chapter 4. Equilibration of hadronic matter: While studying transport coefficient of hadronic matter, it is of importance to consider an equilibrated system. This chapter focuses on studying equilibration of the system by studying chemical equilibrium from particle number density and studying thermal equilibrium through studying particle spectra from energy distribution of the system. The Boltzmann distribution is then used to extract common temperature of the equilibrated state. Hadronic gas model is studied by studying the Equation of State from UrQMD model. The EoS is studied from the evolution

of temperature with pressure and energy density.

In chapter 5. Thermal conductivity transport coefficient: Thermal conductivity transport coefficient is calculated from the heat current - current correlations using the Green-Kubo relations. We study the relationship between the square expectation of heat current, thermal conductivity, the product of thermal conductivity and temperature and relaxation time for heat conductivity with temperature. In chapter 6: Summary and collisions: Here the focus is on the summary of the whole thesis and the conclusion of the study.

Chapter 2

Introduction to Relativistic Kinetic Theory

Relativistic hydrodynamics is an important theoretical tool in heavy-ion physics, astrophysics, and cosmology. Hydrodynamics gives reliable description of the non-equilibrium real-time macroscopic evolution of a given system [22].

The kinetic theory establishes a relationship between macroscopic and microscopic properties, by using a one-particle distribution function $f(x, p)$, where x is the distance between the particles and p is the momentum of the particle. The function $f(x, p)$ describes the phase space density of the particles and the kinetic equation or transport equation governs the time development of $f(x, p)$ [23].

2.1 Basic equations

Now consider a simple system consisiting of relativistic particles of mass m with momentum p and energies cp^0, where p^0 is given as [24]

$$p^0 = \sqrt{p^2 + m^2c^2}. \tag{2.1}$$

The relativistic velocity is defined as

$$\boldsymbol{u} = \frac{cp}{p^0}, \tag{2.2}$$

with momentum p and and c being the speed of light. Some of the tensor notation we considered in this study is four velocity U^μ. With the help of hydrodynamic velocity Eq. (2.2) one may define tensor qauntity [22, 25, 26]

$$\Delta^{\mu\nu}(x) = g^{\mu\nu} - c^{-2}U^\mu(x)U^\nu(x), \tag{2.3}$$

with $g^{\mu\nu}$ the metric tensor given as

$$g^{\mu\nu} = \text{diag}(1, -1, -1, -1). \tag{2.4}$$

throughout the studies. In particular we have

$$p^\mu p_\mu = \left(p^0\right)^2 - p^2 = m^2c^2. \tag{2.5}$$

The convariant Lorentz 4-derivative is defined as

$$(\partial_\mu) \equiv \left(\frac{\partial}{\partial t}, \vec{\nabla}\right) \Leftrightarrow (\partial^\mu) \equiv \left(\frac{\partial}{\partial t}, -\vec{\nabla}\right)^T, \tag{2.6}$$

Where $(.)^T$ denotes a transposed vector.

2.2 Hydrodynamic 4-velocity

The hydrodynamic four-velocity $U^{\mu}(x)$ is an important notion in the description of continuous media. It is defined as a time-like vector with length c in each time-space given as [25]

$$U^{\mu}(x)U_{\mu}(x) = c^2. \tag{2.7}$$

Now taking a first differentiation of Eq. (2.7) with respect to time-space coordinates given as

$$\partial_{\mu} = \frac{\partial}{\partial x^{\mu}} = \left(\frac{1}{c}\partial_t, \nabla\right), \tag{2.8}$$

which yields a useful ancillary relation given as

$$U^{\mu}(x)\partial_{\mu}U_{\mu}(x) = 0, \tag{2.9}$$

With the help of Eq. (2.3) and Eq. (2.4) a projector of four-velocity of $U^{\mu}(x)$ is given as

$$\Delta^{\mu\nu}(x)U^{\nu}(x) = 0. \tag{2.10}$$

In the local rest frame which will be considered in this study and indicated by the inex **LR**, the hydrodynamic four velocity is defined as

$$U^{\mu}_{LR} = (c, 0, 0, 0). \tag{2.11}$$

and the rest frame of the projector defined in Eq. (2.3) has the form [25, 26]

$$\Delta_{LR\mu\nu} = \Delta^{\mu\nu}_{LR} = \mathrm{diag}(0, -1, -1, -1), \quad \Delta^{\mu}_{LR_{\nu}} = \mathrm{diag}(0, 1, 1, 1). \tag{2.12}$$

The knowledge of the above hydrodynamic velocity will be used to discuss various definitions which can be employed such as Eckart's and Landau definitions.

2.2.1 Eckart's definition of four-velocity

The choice made by Eckart's relates the hydrodynamic velocity directly to particle four-flow N^μ by means of definition relation which state that four-velocity is equal to the normalized particle four-flow given as [25]

$$U^\mu = \frac{cN^\mu}{\sqrt{N^\nu N_\nu}}, \tag{2.13}$$

The normalization of the above equation is in agreement with [22, 25, 26][27, 28]. The alternative definition of the above normalized expression is

$$U^\mu = \frac{c^2 N^\mu}{N^\nu U_\nu}. \tag{2.14}$$

Note that a different form of Eq. (2.13) can be obtained by introducing a projector $\Delta^{\mu\nu}(x)$ defined in Eq. (2.3).

$$\Delta^{\mu\nu} N_\nu = 0. \tag{2.15}$$

Eckart's definition implies that in the local rest frame the spatial components of the particle four-flow N^μ vanish [25]

$$N^i_{LR} = 0, \qquad i = 1, 2, 3. \tag{2.16}$$

The hydrodynamic four velocity defined in Eq. (2.13) is known as the mean particle velocity.

2.2.2 Landau and Lifshitz's definition of four-velocity

A different definition of hydrodynamic velocity was proposed by Landau and Lifshitz which is defined as

$$U^{\mu} = \frac{cT^{\mu\nu}U_{\nu}}{\sqrt{U_{\rho}T^{\rho\sigma}T_{\sigma\tau}U^{\tau}}}, \tag{2.17}$$

The above definition of hydrodynamic velocity is related to the flow of energy or one can say to the momentum density [22, 25, 26, 27, 28]. One can still observe that the hydrodynamic velocity U^{μ} is normalized to the speed of light c. The Landau definition defined in Eq. (2.17) can also be written as

$$U^{\mu} = \frac{c^2T^{\mu\nu}U_{\nu}}{U_{\rho}T^{\rho\sigma}U_{\sigma}}. \tag{2.18}$$

With the help of projector $\Delta^{\mu\nu}(x)$ defined in Eq. (2.3), the above definition (2.18) may be formulated as the following condition

$$\Delta^{\mu\nu}T_{\nu\sigma}U^{\sigma} = 0. \tag{2.19}$$

This shows that in the local rest frame associated with the Landau-Lifshitz velocity the momentum density and the energy flow vanish [25]

$$T^{i0}_{LR} = T^{0i}_{LR} = 0, \qquad i = 1, 2, 3. \tag{2.20}$$

Many definitions of hydrodynamic velocity could be investigated, but for this study the focus is only on the above two definitions in which one of the reason is that they are most natural and at least for simple system [25] and they have been discussed quite a number of times.

2.3 Particle four-flow

Consider the two local quantities defined in relativity theory which is the particle density and the particle flow, constitute a four-vector field, and is indicated by

$$N^{\mu}(x) = (cn(x,t), j(x,t)), \tag{2.21}$$

The index μ takes the four values 0, 1, 2 and 3 while $x = x^{\mu} = (ct, x)$ denote a time-space point. With the help of distribution function $f(x,t)$ we define the particle density n as

$$n(x,t) = \int d^3p f(x,p), \tag{2.22}$$

from the particle density the integration is taken over all momenta where by d^3p is the integration element. And the particle flow is define as

$$j(x,t) = \int d^3p \boldsymbol{u} f(x,p), \tag{2.23}$$

Now considering Eq. (2.2) and Eq. (2.22-2.23) one can define particle four-flow as

$$N^{\mu}(x) = c \int \frac{d^3p}{p^0} p^{\mu} f(x,p). \tag{2.24}$$

The last expression in the above equation indicates that the distribution function must be a scalar object [22, 25, 26, 27, 28].

2.4 Energy momentum tensor

Energy per particle is given by cp^0 and the average is written as

$$T^{00}(x) = c\int d^3pp^0 f(x,p), \tag{2.25}$$

where the microscopic energy density is indicated by the symbol T^{00}. From the above equation, one can define energy flow $cT^{0i}(x)$ as follows

$$T^{0i}(x) = \int d^3pp^0 \boldsymbol{u}^i f(x,p) \qquad i = 1,2,3. \tag{2.26}$$

where $i = 1,2,3$ define the cartesian component of velocity $\boldsymbol{u}$. Now lets consider the momentum density which is the average value of the particle momentum p, thus we write $c^{-1}T^{i0}$ as

$$T^{0i}(x) = c\int d^3pp^i f(x,p) \qquad i = 1,2,3, \tag{2.27}$$

Finaly we introduce the momentum flow or also known as pressure tensor which is defined as the flow in the direction $j = 1,2,3$ of the momentum in the direction $i = 1,2,3$ thus

$$T^{ij}(x) = \int d^3pp^i \mathbf{u}^j f(x,p) \qquad i,j = 1,2,3, \tag{2.28}$$

Now lets consider the relation between velocity of the relativistic particle with momentum given in Eq. (2.2), the formulae $(2.25 - 2.228)$ may be written in a way that defines the energy momentum tensor as [22, 25, 26, 27, 28]

$$T^{\mu\nu}(x) = c\int \frac{d^3p}{p^0} p^\mu p^\nu f(x,p), \tag{2.29}$$

with $\mu, \nu = 0, 1, 2, 3$. In the relativistic kinetic theory the energy momentum tensor is defined as the second momentum of the distribution function and thus a symmetric quantity [25] .

2.5 Entropy four-flow

The H-function which was introduced by Boltzmann, implies that the local entropy density for a system outside equilibrium may be defined as [25]

$$c^{-1}S^0(x) = -k_B \int d^3p f(x,p) \left[\log h^3 f(x,p) - 1\right], \tag{2.30}$$

where k_B is Boltzmann's constant and h is an arbitrary constant such that $h^3 f(x,p)$ can be dimensionless [25]. The entropy flow with a particle velocity $\boldsymbol{u}$ that corresponds to the above entropy density is as follows

$$S(x) = -k_B \int d^3p \boldsymbol{u} f(x,p) \left[\log h^3 f(x,p) - 1\right], \tag{2.31}$$

Now consider a relativisitic situation, using Eq. (2.30) and Eq. (2.31) for entropy density and entropy flow and revisiting Eq. (2.2) for relativistic velocity, one can write the four-vector entropy as

$$S^\mu(x) = -k_B c \int \frac{d^3p}{p^0} p^\mu f(x,p) \left[\log h^3 f(x,p) - 1\right]. \tag{2.32}$$

The above expression in Eq. (2.32) is known as the entropy four-flow [22, 25, 26, 27, 28].

2.6 Heat flow

Heat flow is defined as the difference of the energy flow and the flow of enthalpy h "please note that the same symbol h used in Eq. 2.30 is used to define the

enthalpy here" carried by particles [8] and it is given by

$$I_q^\mu = (U_\nu T^{p\sigma} - hN^\sigma)\Delta_\sigma^\nu, \tag{2.33}$$

The enthalpy of the particle h is define as

$$h = e + pn^{-1}, \tag{2.34}$$

with p being the local hydrostatic pressure and hence the pressure tensor is define as

$$P^{\mu\nu} = \Delta_\sigma^\mu T^{\sigma\tau}\Delta_\tau^\mu. \tag{2.35}$$

The pressure it is symmetric quantity when the energy-momentum tensor $T^{\mu\nu}$ is symmetric. From expanding Eq. (2.33) we obtain

$$I_q^\mu = -h\Delta^{\mu\nu}N_\nu + U_\nu T^{\nu\sigma}\Delta_\sigma^\mu, \tag{2.36}$$

where the first term is known as the **Eckart's heat flow**

$$I_q^\mu = U_\nu T^{\nu\sigma}\Delta_\sigma^\mu, \tag{2.37}$$

The second term from the above equation is known as **Landau-Lifshitz heat flow**

$$I_q^\mu = -h\Delta^{\mu\nu}N_\nu. \tag{2.38}$$

Note that the Eckart's and Landau-Lifshitz hydrodynamic four-velocities are defined in section (2.2) subsection (2.2.1) and subsection (2.2.2) respectively.

Chapter 3

Short description of the UrQMD model

3.1 Introduction

This chapter focuses on how the model is used to simulate the ultra-relativistic heavy ion collisions. To study how the collisions between particles are initialized inside the model using the input file and what are the parameters required for the initialization. The results produced during collisions which are stored in the output file will then be used to study thermal conductivity transport coefficient of the meson gas.

3.2 Ultra-relativistic Quantum Molecular Dynamics

The UrQMD model was developed by the theorists at Frankfurt in Germany. It intends to provide a unified description of various aspects of nuclear reactions. It describes the phenomenology of the hadronic interactions from few hundreds MeV up to the newly LHC energy of $\sqrt{s}$ =14 TeV per nucleon in the centre of mass system [8, 14, 29, 30].

The model is used to simulate collisions between the proton+proton, the proton+nucleus, and the nucleus+nucleus interaction at different energies per nucleon [30]. The UrQMD is a microscopic model based on a phase space description of the nuclear reactions. It has been designed to analyse the physics of the excitation function of hadronic abundances, stopping and the flow [31].

The UrQMD hybrid model has been developed in the past years to combine the advantages of the hadronic transport theory and the ideal fluid dynamics in order to provide a major step forward as compared to the simplified expanding fireball models employed so far [32]. It provides a realistic and well established background, including the event-by-event fluctuations and has been shown to describe well many collective properties of the relativistic heavy-ion collision [32].

3.3 Relativistic transport equation used in the UrQMD model

In this section we consider a relativistic case which is applicable to the model we are using to simulate ulra-relativistic heavy ion collision known as UrQMD model. To derive this relativistic transport equation one starts from an effective Langrangian with baryons and mesons as elementary degrees of freedom. Consider the Lagrangian density for nucleons, deltas and a nucleon resonance like N^*_{1440} plus the σ, ω and π meson. The Lagrangian reads [6]

$$\begin{aligned}\mathcal{L}_F = &\bar{\psi}\left[i\gamma_\mu\partial^\mu - M_N\right]\psi \\ &+ \bar{\psi^*}\left[ii\gamma_\mu\partial^\mu - M_N\right]\psi^* + \bar{\psi_{\Delta_\nu}}\left[i\gamma_\mu\partial^\mu - M_\Delta\right]\psi^\nu_\Delta + \frac{1}{2}\partial_\mu\sigma\partial^{\mu\sigma} - U(\sigma) \\ &- \frac{1}{4}\omega_{\mu\nu}\omega^{\mu\nu} + U(\omega) + \frac{1}{2}\left(\partial_\mu\pi\partial^\mu\pi - m^2_\pi\pi^2\right), \quad (3.1)\end{aligned}$$

and $U(\sigma)$, $U(\omega)$ are the self-interaction part of the scalar field and vector field

$$U(\sigma) = \frac{1}{2}m^2_\sigma\sigma^2 + \frac{1}{3}b\left(\mathrm{g}^\sigma_{NN}\sigma\right)^3 + \frac{1}{4}c\left(\mathrm{g}^\sigma_{NN}\sigma\right)^4, \quad (3.2)$$

and

$$U(\omega) = \frac{1}{2}m^2_\omega\omega_\mu\omega^\mu\left(1 + \frac{\left(\mathrm{g}^\omega_{NN}\right)^2}{2}\frac{\omega_\mu\omega^\mu}{Z^2}\right), \quad (3.3)$$

respectively $\mathcal{L}_I$ is the interaction Lagrangian density

$$\mathcal{L}_I = \mathcal{L}_{NN} + \mathcal{L}_{N^*N^*} + \mathcal{L}_{\Delta\Delta} + \mathcal{L}_{NN^*} + \mathcal{L}_{\Delta N} + \mathcal{L}_{\Delta N^*}, \quad (3.4)$$

$$\mathcal{L}_I = \mathrm{g}^A_{NN}\bar{\psi}(x)\Gamma^N_A\psi(x)\Phi_A(x) + \mathrm{g}^A_{N^*N^*}\bar{\psi}^*(x)\Gamma^{N^*}_A\psi(x)\Phi_A(x)$$
$$+ \mathrm{g}^A_{\Delta\Delta}\psi_{\Delta\nu}(x)\Gamma^\Delta_A\psi^\nu_\Delta(x)\Phi_A(x)\left[\mathrm{g}^A_{NN^*}\bar{\psi}^*(x)\Gamma^{N^*}_A\psi(x)\Phi_A(x)\right]$$
$$- \mathrm{g}^A_{\Delta\Delta}\psi_{\Delta\nu}(x)\Gamma^\Delta_A\psi^\nu_\Delta(x)\Phi_A(x)\left[\mathrm{g}^\pi_{\Delta N}\bar{\psi}_{\Delta\mu}(x)\partial^\pi\pi(x).\mathbf{S}^+\psi(x)\right]$$
$$- \mathrm{g}^A_{\Delta\Delta}\psi_{\Delta\nu}(x)\Gamma^\Delta_A\psi^\nu_\Delta(x)\Phi_A(x)\left[\mathrm{g}^\pi_{\Delta N^*}\bar{\psi}_{\Delta\mu}(x)\partial^\pi\pi(x).\mathbf{S}^+\psi(x)^* + h.c.\right]. \quad (3.5)$$

Here, ψ, ψ^* are the Dirac spinors of the nucleon and $N^*(1440)$, and $\psi_{\Delta\mu}$ is the Rarita-Schwinger spinor of the Δ-baryon. $\mathrm{g}^\pi_{\Delta N} = f^*/m_\pi$; $\Gamma^N_A = \Gamma^{N^*}_A = \gamma_A\tau_A$, $\Gamma^\Delta_A = \gamma_A T_A$, $A = \sigma, \omega, \pi$, more about the above Lagrangian and meaning of the symbols can be found in [6] An example of the RBUU equation for the nucleons, N^*_{1440} distribution function now reads [6]

$$C^{N^*}(x,p) =$$
$$\left\{p_\mu\left[\partial^\mu_x - \partial^\mu_x\Sigma^\nu_{N^*}(x)\partial^p_\nu + \partial^\nu_x\Sigma^\mu_{N^*}(x)\partial^p_\nu\right] + m^*_{N^*}\partial^\nu_x\Sigma^S_{N^*}(x)\partial^p_\nu\right\}\frac{f_{N^*}(X,P,t)}{E^*_{N^*}(p)}. \quad (3.6)$$

The collision term on the r.h.s can be written as

$$C^{N^*}(x,p) = \frac{1}{2}\int\frac{d^3p_2}{(2\pi)^3}\int\frac{d^3p_3}{(2\pi)^3}\int\frac{d^3p_4}{(2\pi)^3}(2\pi)^4\delta^4(p+p_2-p_3-p_4)$$
$$\times W^{N^*}(p,p_2,p_3,p_4)(F_2-F_1), \quad (3.7)$$

Where F_2, F_1 are the Uehling-Uhlenbeck factors [6, 23]

$$F_2 = [1-f_{N^*}(X,P,t)][1-f_{B_2}(X,P,t)]f_{B_3}(X,B,t)f_{B_4}(X,P,t), \quad (3.8)$$

$$F_1 = f_{N^*}(X,P,t)f_{B_2}(X,P_2,t)[1-f_{B_3}(X,P_3,t)][1-f_{B_4}(X,P,t)], \quad (3.9)$$

And $W^{N^*}(p, p_2, p_3, p_4)$ is the transition probability for different channels.

$$W^{N^*}(p, p_2, p_3, p_4) = \frac{1}{16 E^*_{N^*}(p)\, E^*_{B_2}(p_2)\, E^*_{B_3}(p_3)\, E^*_{B_4}(p_4)} \Sigma_{AB} \left(T_D \Phi_D - T_E \Phi_E\right) + p_3 \longleftrightarrow p_4. \quad (3.10)$$

Here T_D, T_E are the isospin matrices and Φ_D, Φ_E are the spin matrices, respectively. D denotes the contribution of the direct diagrams and E is that of the exchange diagrams. A, $B = \sigma$,ω,π represent the contributions of different mesons. The exchange of momentum p_3 and p_4 is only for the case of identical particles in the final state. A full explanation about the above derivation can be found at [6].

3.4 Initialization

This section describes the initialization of the projectile and the target nuclei in the UrQMD model. The projectile and the target nuclei are modeled according to the Fermi-gas ansatz [6, 30]. The wave function of nucleus is defined as the product of the wave-function of the single nucleon Gaussian. Therefore, each nucleon is represented by the coherent state Eq. 3.11 of the form [6, 30]

$$\varphi_j(\boldsymbol{x}_j, t) = \left(\frac{2\alpha}{\pi}\right)^{\frac{3}{4}} \exp\left\{-\alpha \left(\boldsymbol{x}_i - \boldsymbol{r}_j(t)\right)^2 + \frac{i}{\hbar} \boldsymbol{p}_j(t) \boldsymbol{x}_j\right\}. \quad (3.11)$$

The above formula is characterized by 6 time-dependent parameters, q_i and p_i, respectively and parameter L is related to the extension of the wave packet in phase space, and it is fixed [30]. The wave function is assumed to be the direct product of coherent state given by

$$\Phi = \prod_j \varphi_j(\boldsymbol{x}_i, \boldsymbol{p}_i, t). \quad (3.12)$$

Each initialized nucleus must meet the following constraints

• $\sum_i \boldsymbol{q}_i = \mathbf{0}$, i.e. it is a centred in the configuration space around $\mathbf{0}$,

• $\sum_i \boldsymbol{v}_i = \mathbf{0}$, i.e. the nucleus is at rest,

• its binding energy should correspond to the value given by the Bethe-Weizsäcker formula,

• the radius should yield the following mass dependence of R(A) $\sim r_0.\mathrm{A}^{\frac{1}{3}}$ and have a reasonable surface-thickness,

• in its centre, nucleus should have the nuclear matter ground-state density.

In configuration space the centroids of the Gaussians are randomly distributed within a sphere with radius R(A) [6, 30]

$$R(A) = r_0 \left(\frac{1}{2} \left[A + \left(A^{\frac{1}{3}} - 1 \right)^3 \right] \right)^{\frac{1}{3}}, \qquad r_0 = \left(\frac{3}{4\pi\rho_0} \right)^{\frac{1}{3}}. \tag{3.13}$$

The parameter r_0 is a function of a nuclear matter ground state density ρ_0 used in the UrQMD model [6, 30, 33]. Due to the relatively small number of nucleons to be distributed over a volume of nucleus may result in large fluctuations in the mean density of nucleus, thus the phase-space density at the location of each nucleon is evaluated after its placement [6]. If the phase-space is too high (i.e. the respective area of the nucleus is already occupied by other nucleons), then the location of that nucleon is rejected and the new location is randomly chosen [6, 30]. The initial momenta of nucleons are randomly chosen between 0 and the local Thomas-Fermi-momentum

$$p_F^{max} = \hbar c \left(3\pi^3 \rho \right)^{\frac{1}{3}}, \tag{3.14}$$

with ρ being the corresponding local proton-density or neutron-density. More about the initialization including the principal disadvantage of the above intial-

ization can be found in [6, 30].

3.5 The collision term

The UrQMD collision term contains 55 different baryon species and 32 meson species which are supplemented by their corresponding anti-particle and all the isospin-projected states [6, 29, 31]. The baryons and baryon-resonances which can be populated in the UrQMD are listed in the table 3.2 together with the respective mesons and meson-resonances listed in table 3.1. The states listed can either be produced in string decays, s-channel collisions or resonance decays [6].

The elementary cross sections are fitted to the available proton-proton or the pion-proton data. The isospin symmetry is used when possible in order to reduce the number of individual cross-sections which have to be parameterized or tabulated [6].

In the UrQMD model the hadron-hadron collisions are performed stochastically and the cross section is interpreted geometrically as an area. A collision between two hadrons will occur if

$$d_{trans} \leq \sqrt{\frac{\sigma_{tot}}{\pi}}, \qquad \sigma_{tot} = \sigma(\sqrt{s}, type), \tag{3.15}$$

where d_{trans} and σ_{tot} are the impact parameter of hadrons and total cross-section of two hadrons, respectively [29]. In the UrQMD model the total cross-section σ_{tot} are a function of the incoming and outgoing particle types and depends on the isospins of the colliding particles, their flavour and the centre-of-mass (c.m) energy $\sqrt{s}$. More details about the UrQMD model is presented in [6, 29, 30].

Table 3.1 represent all the mesons and meson-resonances, sorted with respect to their spin and their parity included in the UrQMD model. The mesons in table 3.1 that will be used for this study are pion denoted by the symbol (π), rho denoted by the symbol (ρ) and kaon denoted by the symbol (K). Table 3.2 represent all the baryons and baryon-resonances included in the UrQMD model.

0^{-+}	1^{--}	0^{++}	1^{++}	1^{+-}	2^{++}	$(1^{--})^{*}$	$(1^{--})^{**}$
π	ρ	a_0	a_1	b_1	a_2	ρ_{1450}	ρ_{1700}
K	K^*	K_0^*	K_1^*	K_1	K_2^*	K_{1410}^*	K_{1680}^*
η	ω	f_0	f_1	h_1	f_2	ω_{1420}	ω_{1662}
η'	ϕ	f_0^*	f_1'	h_1'	f_2'	ϕ_{1680}	ϕ_{1900}

Table 3.1: The mesons and meson-resonances, sorted with respect to their spin and their parity included in the UrQMD model [34].

nucleon	delta	lambda	sigma	xi	omega
N_{938}	Δ_{1232}	Λ_{1116}	Σ_{1192}	Ξ_{1315}	Ω_{1672}
N_{1440}	Δ_{1600}	Λ_{1405}	Σ_{1385}	Ξ_{1530}	
N_{1520}	Δ_{1620}	Λ_{1520}	Σ_{1660}	Ξ_{1690}	
N_{1535}	Δ_{1700}	Λ_{1600}	Σ_{1670}	Ξ_{1820}	
N_{1650}	Δ_{1900}	Λ_{1670}	Σ_{1750}	Ξ_{1950}	
N_{1675}	Δ_{1905}	Λ_{1690}	Σ_{1775}	Ξ_{2030}	
N_{1680}	Δ_{1910}	Λ_{1800}	Σ_{1915}		
N_{1700}	Δ_{1920}	Λ_{1810}	Σ_{1940}		
N_{1710}	Δ_{1930}	Λ_{1820}	Σ_{2030}		
N_{1720}	Δ_{1950}	Λ_{1830}			
N_{1900}		Λ_{1890}			
N_{1990}		Λ_{2100}			
N_{2080}		Λ_{2110}			
N_{2190}					
N_{2200}					
N_{2250}					

Table 3.2: The baryons and baryon-resonances included into the UrQMD model. Though the baryon-antibaryon symmetry and the respective antibaryon state are included as well [34].

3.6 The input file and The output file

Now one has an idea about how the nuclei and particles in the model collide and interact amongst each other, how the projectile and target nuclei are initialized, what are the impact parameters and what are those particles included in the model.

In this section the focus is on how to use this model to simulate ultra-relativistic heavy ion collision through studying two types of input files, namely (1) the sample input file for urqmd: used for the nucleus+nucleus collisions and (2) the infinite matter (box) calculations: used to simulate the ultra-relativistic collisions between the particles in a cubic box with the periodic boundary conditions [35]. The results produced during the collisions are recorded in the output file and then used for various studies. For this study the results are used to study equilibration of hadron gas, EoS and to study the transport coefficient namely thermal conductivity transport coefficient. More details about the input and output file can be found in Appendix A and B.

Chapter 4

Equilibration of hadronic matter

4.1 Introduction

To investigate the equilibrium of a system, a microscopic calculation using the UrQMD model is used to simulate the ultra-relativistic heavy ion collision. A multi-particle production plays an important role in the equilibration of the hadrons gas [5]. To study the equilibration a system of cubic box which impose the periodic boundary conditions in the configuration space is used [3, 5]. This simply means that if a particle leaves the box another particle with the same momentum enters the box from the opposite side.

The energy density ε, volume V and the baryon number density n_B in the box are fixed as input parameters and are conserved throughout the simulation. The energy density is defined as $\varepsilon = \frac{E}{V}$, where E is the energy of N particles given by

$$E = \sum_{i=1}^{N} \sqrt{m_i^2 + p_i^2}, \tag{4.1}$$

and the three-momenta p_i of the particles in the initial state are randomly distributed in the centre of mass system of the particles that is

$$\sum_{i=1}^{N} p_i = 0. \tag{4.2}$$

The time evolution of the particles is described by the UrQMD. We consider time evolutions of the particle densities and the energy distributions of different meson species.

To investigate the equilibration phenomena of the system this chapter is divided into the following sections. In section (4.2) we study the chemical equilibration: this is done by extracting the particle number densities of the different meson species with time. In section (4.3) we study the thermal equilibrium and temperature: this is done by studying the energy distributions of different light meson species by studying the particle spectra and using the Boltzmann distribution to extract common temperatures of the system. In section (4.4) we study the hadronic gas model: this is done by studying the Equation of State (EoS) of the UrQMD model through studying the evolution of temperature (T) with the energy density ε and the pressure P. The system tends towards equilibrium state when time and energy density increases as shown in the results.

4.2 Chemical equilibrium

In this section the chemical equilibrium is studied from the particle number densities of different light meson species in a box with $V = 1000$ fm^3, zero net baryon number density $n_B = 0.0$ fm^{-3} at different energy densities from $\varepsilon = 0.3$ GeV/fm^3 using UrQMD box calculations.

The ideal hadron gas models have been used to describe the particle abundances and energy spectra from the central heavy-ion reactions at both AGS and SPS energies. Therefore in this model the system is described by a grand canonical ensemble of non-interacting fermions and bosons in equilibrium at a temperature T [14]. The particle multiplicity is given as

$$N_i = \frac{g_i V}{(2\pi)^3} \int_0^\infty \frac{4\pi p^2 dp}{\exp\left[\left(E_i - B_i\mu_B - S_i\mu_S\right)/T\right] \pm 1}, \tag{4.3}$$

where g_i is the spin-isospin degeneracy factor of the particle i. The E_i, B_i and S_i are the single particle energy, baryon number and the strangeness, and μ_B and μ_S are the baryon and the strangess chemicla potentials [14, 36].

Figure 4.1 to 4.3 represent the time evolution of the various meson (π, ρ, K) number densities at different energy densities $\varepsilon = 0.2$, 0.3 and 0.4 GeV/fm^3. The meson species reached equlibrium state when time increases. It is observed that the pions have a large amount of particle number densities and the reason could be the decay in the heavier mesons and other particles produced in the system to form the pions.

The saturation of the particle number densities in figure 4.1 to 4.3 indicate the realization of the local equilibrium of the meson species, and thus as conclusion, the chemical equilibrium of the system has been reached. In figures 4.1 to 4.3 the results obtained where very small thus formula (4.4) is used to rescale those results for better analysis of the results and for much readable plots

$$n = \frac{n_{\pi,\rho,K} \times L_{\pi,\rho,K}}{V \times N_{events}}, \tag{4.4}$$

where $n_{\pi,\rho,K}$ is the particle number density (fm^{-3}) for each meson considered in this UrQMD model and $L_{\pi,\rho,K}$ is the scailing factor for each meson. In this calculation $L_\pi = 1$ fm^3, $L_\rho = 200$ fm^3, $L_K = 100$ fm^3 and $N_{evebts} = 200$.

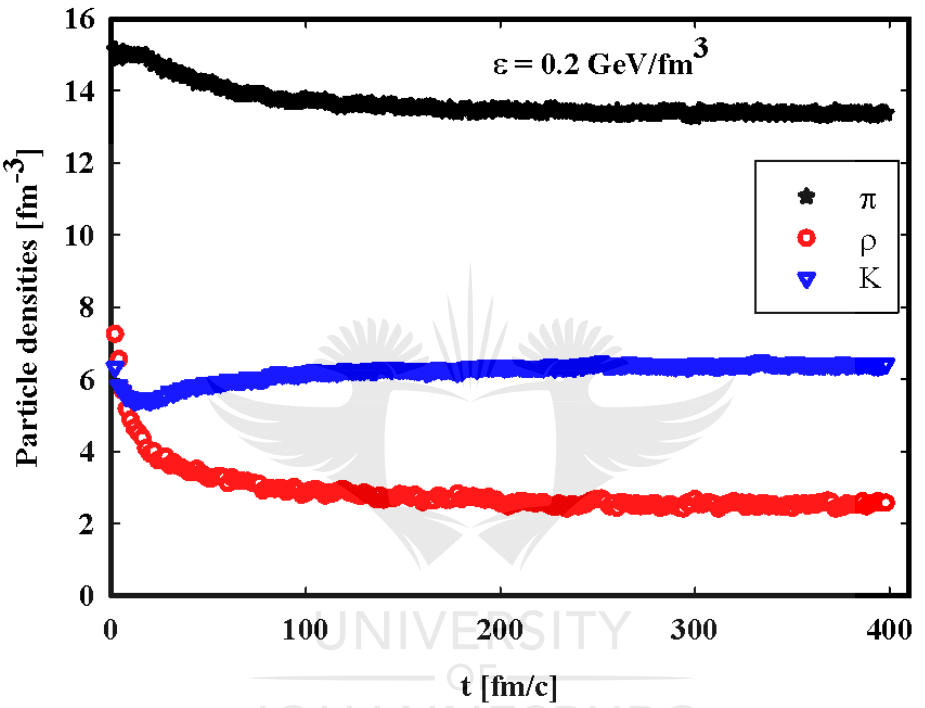

Figure 4.1: The time evolution of particle number densities of light meson species, (π, ρ and K) at $\varepsilon = 0.2$ GeV/fm^3.

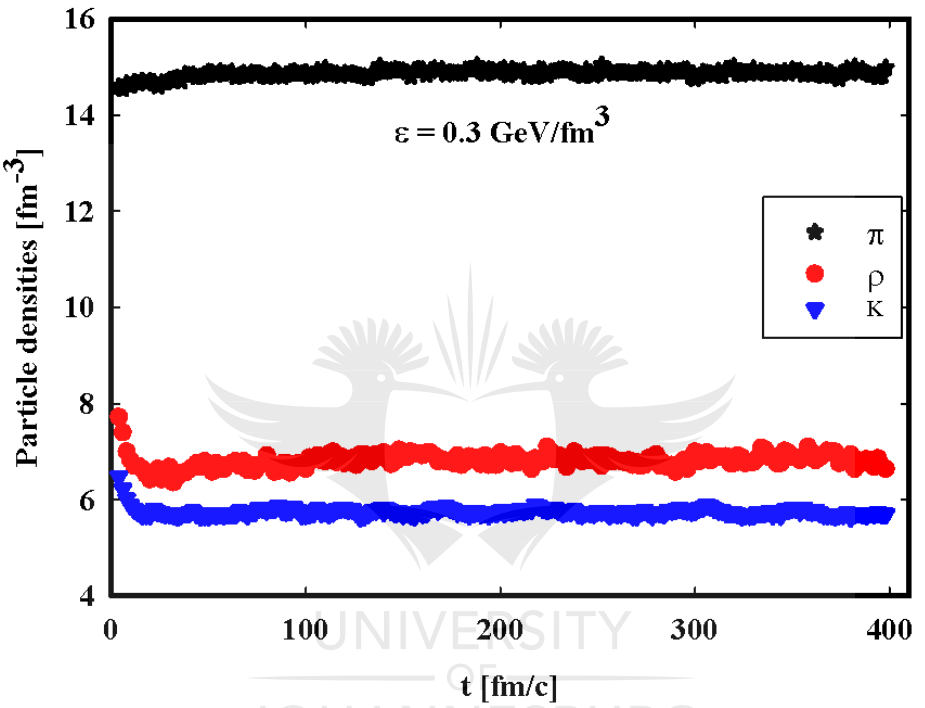

Figure 4.2: The time evolution of particle number densities of light meson species, (π, ρ and K) at $\varepsilon = 0.3$ GeV/fm^3.

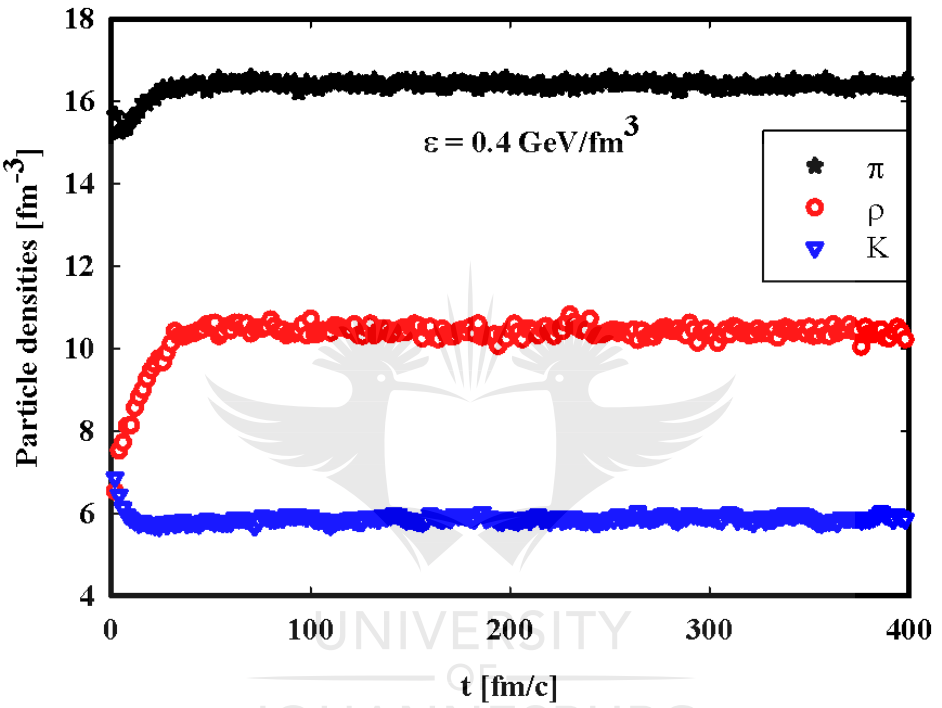

Figure 4.3: The time evolution of particle number densities of light meson species, (π, ρ and K) at $\varepsilon = 0.4$ GeV/fm^3.

In figure 4.1 where $\varepsilon = 0.2$ GeV/fm^3 it is observed that not much of the particle multiplicity took place. The less energy inside the periodic box infuence less production of the particle multiplicity due to a low interaction between the particles. The paticle density of the π and ρ decreases to equilibrium state. The K decreases slightly and then increases its equilibrium state. A difference in the manner that the particles reaches their equilibrium state might be influenced by different life-time of these particles and the decay of other particles to form others inside the box. In figure 4.1 the equilibrium time for all meson species is around $t = 17$ fm/c.

In figure 4.2 where $\varepsilon = 0.3$ GeV/fm^3 the rhos and kaons particles decrease to their equilibrium state while pions quickly reach equilibrium state and never decreases. This is because lot of the particles are now produced during collision due to the increase in the energy inside the box and most of those particle decays to form pion. The equilibrium time for this energy density is around $t = 22$ fm/c.

In figure 4.3 where the energy density $\varepsilon = 0.4$ GeV/fm^3 is even high, a change of shape is observed for these meson species where by the pions and rhos increase to equilibrium state while the kaon still decreases to equilibrium state. The results show that when the energy density increases inside the box, the particle multiplicity also increases. The equilibrium time for this energy density increases to $t = 32$ fm/c.

In the above figures 4.1 - 4.3 it is observed that chemical equilibrium is reached at different values of time and the particle number densities for all the different energy densities. It is observed that for each and every energy density the chemical equilibrium is reached below $t = 100$ fm/c. From $\varepsilon = 0.2 - 0.4$

GeV/fm^3 the saturation of the meson species change shapes with increasing energy densities. These results do make sense as one would expect the particle multiplicity to be less at lower energy density and increases when the energy densities increases. Thus one can say that energy density initialized in the box influences particle production and multiplicity. The chemical equilibration of the pions is always greater than other particles due to the decay of heavier mesons to form pions. In conclusion, particles chemical equilibrium at different energy densities has been reached.

4.3 Thermal equilibrium and temperature

In section 4.2 we study the chemical equilibrium through extracting particle number density of different meson species. We were able to obtain the equilibrium state. From saturation of particle number densities of different meson species, we concluded that chemical equilibrium has been realized thus we move our focus to study the second equilibration stage.

In this section the thermal equilibrium and the temperature from the energy distributions of different light meson species are studied. The possibility of the thermal equilibrium of the hadronic matter is studied by examining the energy distribution of the system in a box with periodic boundary conditions using UrQMD model. The particle spectra is given by the momentum distribution as

$$\frac{dN_i}{d^3p} = \frac{dN}{4\pi E p dE} \propto Ce^{(-\beta E_i)}. \tag{4.5}$$

Figures 4.4 to 4.6 represent the time evolution of energy spectra of different meson species at different energy densities $\varepsilon = 0.025 - 2$ GeV/fm^3 . The

linear lines are fitted using the Boltzmann distribution which is aproximated by $C\exp(-\beta E_i)$ from Eq. (4.5) where $\beta = 1/T$ is the slope parameter of the distribution and E_i is the energy of particle i.

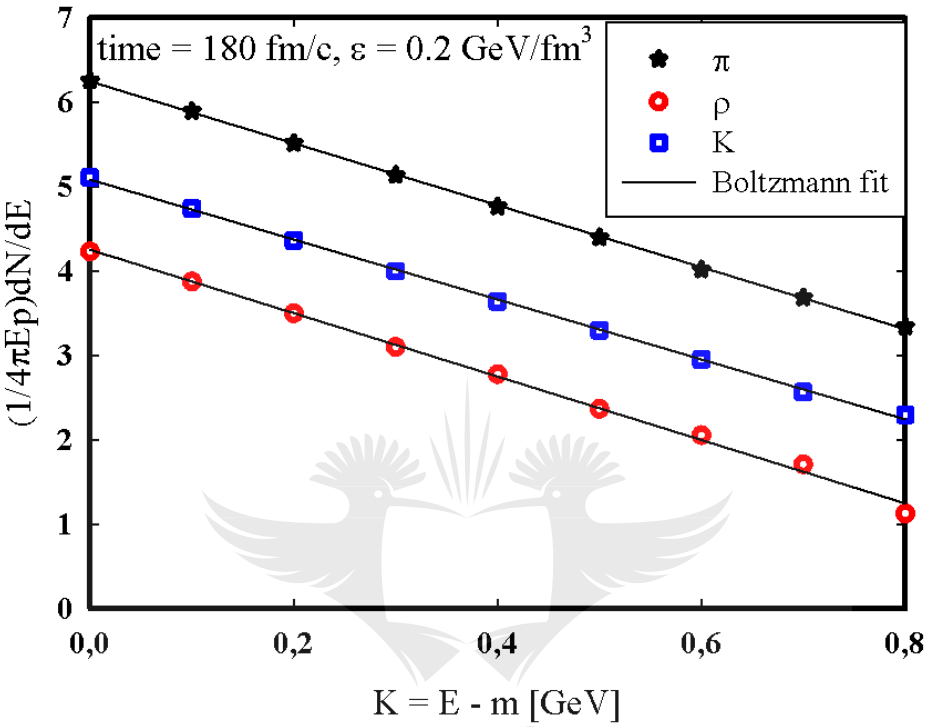

Figure 4.4: The energy distributions of the π, the ρ and the K at $\varepsilon = 0.2$ GeV/fm^3 and $t = 180$ fm/c. The lines are the Boltzmann fit which gives the extracted temperature of $T = 118.3$ MeV.

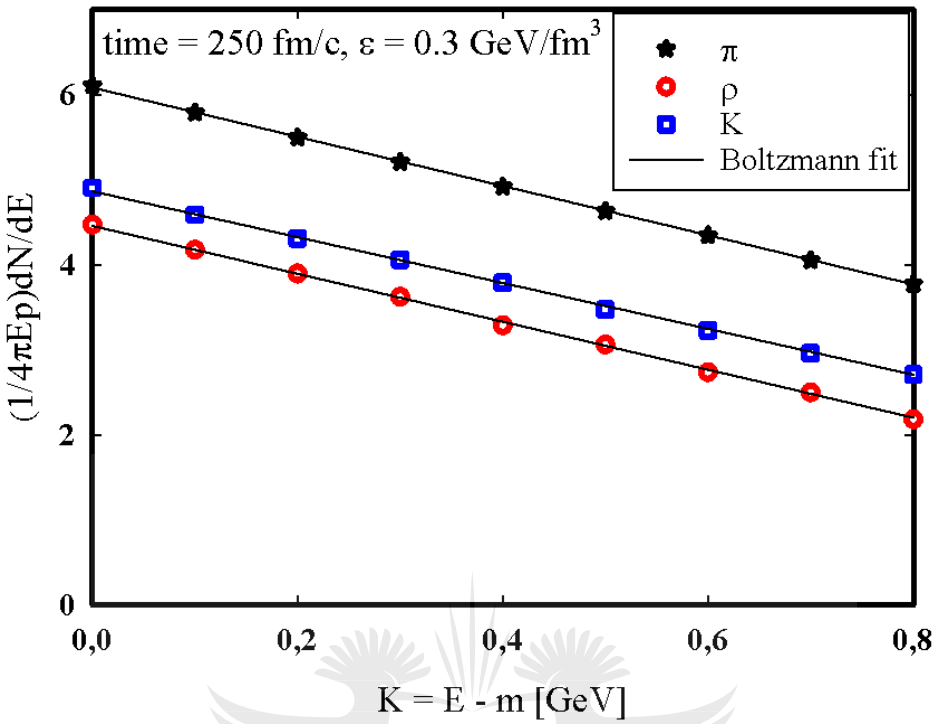

Figure 4.5: The energy distributions of the π, the ρ and the K at $\varepsilon = 0.3$ GeV/fm^3 and $t = 250$ fm/c. The lines are the Boltzmann fit which gives the extracted temperature of $T = 150.1$ MeV.

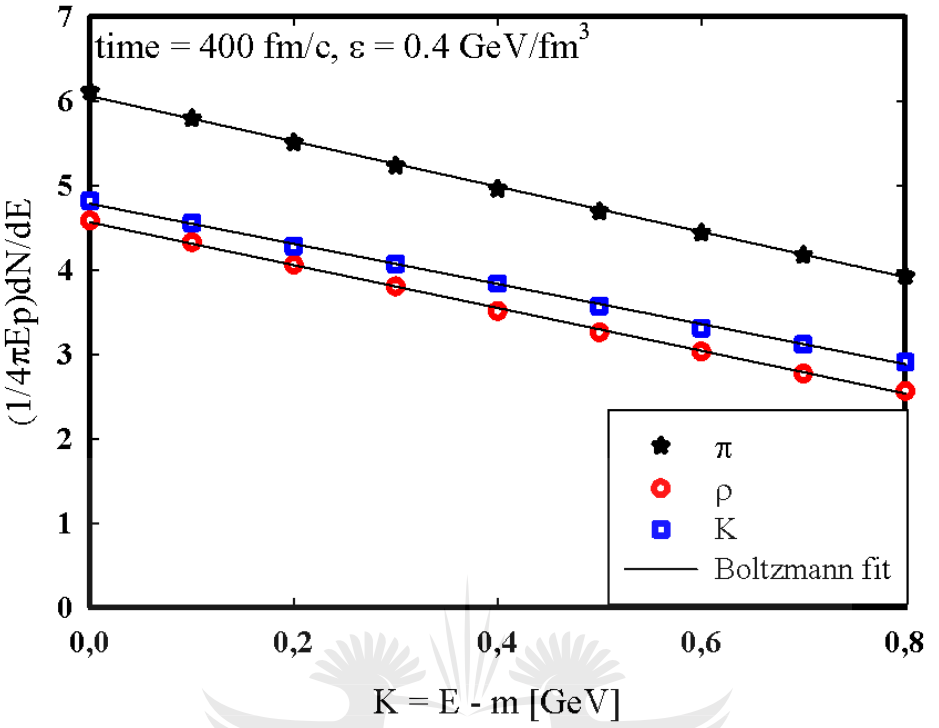

Figure 4.6: The energy distributions of the π, the ρ and the K at $\varepsilon = 0.4$ GeV/fm^3 and $t = 400$ fm/c. The lines are the Boltzmann fit which gives the extracted temperature of $T = 155.01$ MeV.

Figure 4.4 and figure 4.6 represent the energy spectra of meson species namely the pion, the kaon and the rho particles produced during the ultra-relativistic heavy ion collisions simulated using the UrQMD model in a box. The results are plotted as a function of kinetic energy $K = E - m$, so that the horizontal axes for all the particle species coincide [37]. The figures were produced at different energy densities respectively, with $\varepsilon = 0.2$ GeV/fm^3 for figure 4.4, $\varepsilon = 0.3$ GeV/fm^3 for figure 4.5 and $\varepsilon = 0.4$ GeV/fm^3 for figure 4.6. and time. The line represents Boltzmann distribution fit which was used to extract common temperature T coefficients at different energy densities.

It is observed that when we increase energy densities the temperature increases too. Energy spectra of pion is larger than the other because during collision inside the periodic box, other meson species decay to form pions. The temperature we extracted is between $T = 90$ - 170 MeV because thats the region where hadron gas is to be realized in the central high energy collision and this studies only focus on the thermal conductivity of hadron gas made out of meson and zero baryon number density.

From the figures 4.4 to 4.6 it is observed that the slopes of the energy distribution converges to common value of temperatures at different times, above $t = 180$ fm/c for $\varepsilon = 0.2$ GeV/fm^3, above $t = 250$ fm/c for $\varepsilon = 0.3$ GeV/fm^3 and above $t = 400$ fm/c for $\varepsilon = 0.4$ GeV/fm^3. The difference in equilibrium time indicates that the system tends to take long time to equilibrate when energy densities inside the box increases. It is observed that when energy density increases, particles tend to equilibrate closer to each other as shown in figure 4.6.

In thermal equilibrium the system is characterized by unique temeperature

T [37] thus we obtained the thermal temperatures to be $T = 118.3$ MeV for $\varepsilon = 0.2$ GeV/fm^3, $T = 150.1$ MeV for $\varepsilon = 0.3$ GeV/fm^3 and $T = 155.0$ MeV for $\varepsilon = 0.4$ GeV/fm^3. These temperatures extracted from thermal equilibrium using the Boltzmann distribution at different energy densities $\varepsilon = 0.1$ - 0.5 GeV/fm^3 will be used to study EoS as well as the thermal conductivity transport coefficient. The results obtained in figures 4.4 to 4.6 whereby the slopes of all three meson converges to common value of temperatures $T = 118.3$ MeV for figure 4.4, $T = 150.1$ MeV for figure 4.5 and $T = 155.0$ MeV for figure 4.6 at different energy densities and time indicate the realization of the thermal equilibrium.

4.4 Hadronic Gas model (EoS)

In section 4.3 we study thermal equilibrium and temperature of different meson species included in the UrQMD box calculations. We then extracted common temperatures at different energy densities in an equilibrium state. It was observed that temperature increases with increase in energy densities.

In this section we will study the relationship between the temperatures extracted in section 4.3 with the energy densities and pressure by studying hadronic gas model. The intriguing possibilities of phase transitions at various orders in the nuclear Equation of State (EoS), i.e. the relationship specifying how the pressure or alternatively the energy per particle depend on the energy density and temperature is of fundamental interest [38, 39]. It has long played a central role in heavy-ion physics from intermediate to very high energies [14]. The equation of state of hot and dense hadron gas have been investigated using UrQMD and this work has provided valuable information regarding the nature of the hadron gas.

The hadron abundances and the ratios have been suggested as the possible signatures for the exotic states and the phase transitions of the nuclear matter [40]. These signatures have been applied to the study of the chemical equilibration in the relativistic heavy ion reactions. The properties like the temperatures, entropies and the chemical potentials of the hadronic matter have been extracted assuming thermal and chemical equilibrium [29].

The equation of state can be studied using a statistical model which is described by the grand canonical ensemble of a non-interacting hadrons in an equilibrium state at temperature T as presented in [5, 6].

A large number of studies have been done to study EoS of hadron gas [5, 6, 14, 41]. For this study the focus is only on the EoS of hadron gas made out of the π, the ρ and the K calculated from the UrQMD model. This is done through studying the evolution of pressure and energy density with temperature.

$$\varepsilon = \frac{1}{V} \sum_{i=1}^{all-particles} E_i \,, \tag{4.6}$$

and the pressure which is given by

$$P = \frac{1}{3V} \sum_{i=1}^{all-particles} \frac{p_i^2}{E_i}. \tag{4.7}$$

Figure 4.7 and figure 4.8 represent the EoS of hadronic matter namely the pressure and energy density as function of temperature. The energy density used here is the same energy density used as an input parameter during the initialization of the ultra-relativistic heavy ion collision in the UrQMD. The pressure is then calculated from the collision results using Eq. (4.7). The thermal temperatures used here are extracted from the thermal equilibrium in section 4.4 using the Boltzmann distribution function given as $C\exp(-\frac{E}{T})$.

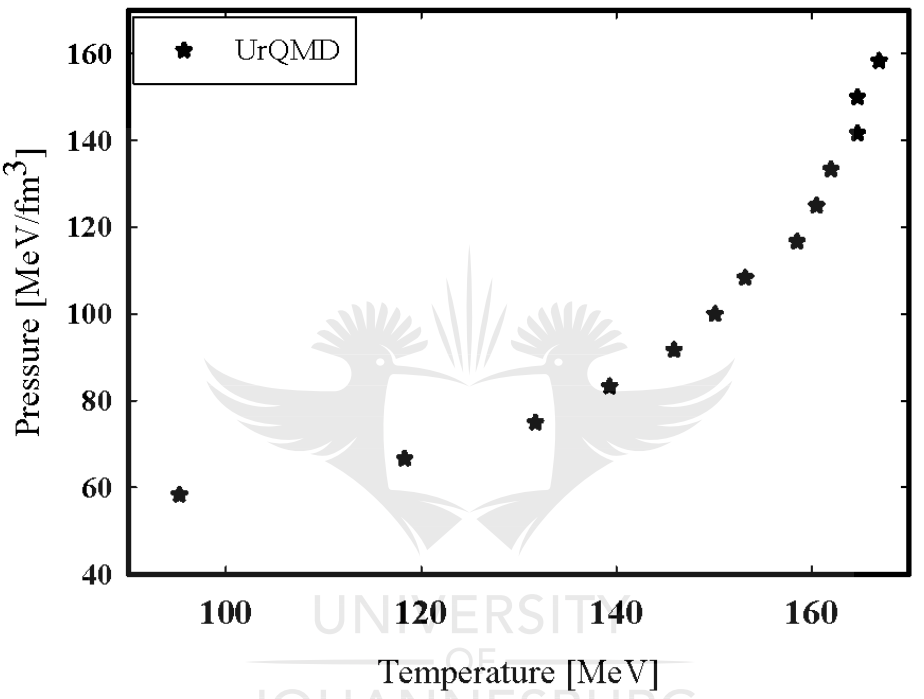

Figure 4.7: Equation of state of a mixed hadron gas of the π, the ρ and the K at a finite temperature (100 MeV $< T <$ 200 MeV). Pressure of the hadronic gas is plotted as a function of a temperature.

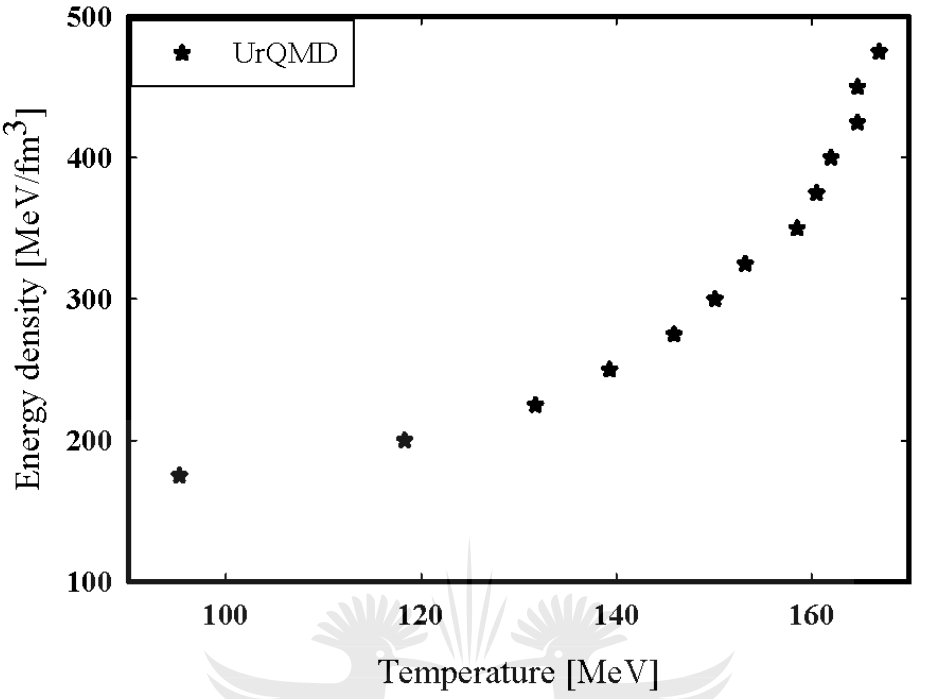

Figure 4.8: Equation of state of a mixed hadron gas of the π, the ρ and the K at finite temperature (100 MeV $< T <$ 200 MeV). Energy density of hadronic gas is plotted as a function of temperature.

From the above figure 4.7 and figure 4.8, both pressure and energy density increases with an increase in the temperature. The results are in good comparison with those obtained in [5, 6].

The focus is on the hadronic scale temperature of (100 MeV $< T <$ 200 MeV) and the zero baryon number density which is expected to be realized in the central high energy nuclear collisions [5]. The pressure and energy density grows with temperature.

In figure 4.7 and figure 4.8 at low temperatures between $T = 90$ MeV to $T = 150$ MeV the power law T^2 of hadron gas behaves differently than the power law T^4 at high temperature between $T = 155$ MeV to $T = 170$ MeV.

This results conclude that one can only calculate the thermal conductivity of this system between 100 MeV and 160 MeV as above 160 MeV while the temperature increases the system start to behave like that of massless particles called QGP. The above results in figure 4.7 and figure 4.8 show that the pressure and the energy density increases exponentially with temperature.

Chapter 5

Thermal conductivity transport coefficient.

5.1 The Green-Kubo formalism and the thermal conductivity transport coefficient

The transport coefficients such as the thermal conductivity κ and the shear viscosity η characterize the dynamics of the fluctuations of the dissipative fluxes in a medium [5]. The most often used method to investigate these coefficient is either through employing the kinetic theory or the field theory using the Green-Kubo formula [5].

The Green-Kubo relations is used for calculation of transport coefficients of shear viscosity, thermal conductivity, thermal diffusion and mutual diffusion for a binary mixture of hard spheres as well as for the calculation of diffusion coefficient of a hadron [4, 5, 18, 42].

A knowledge of various transport coefficients is important for the dissipative

fluid dynamical model. One can calculate the coefficient of thermal conductivity from the fluctuation-dissipative theorem. The fluctuation-dissipative theorem tells us that the thermal conductivity is given by the heat current-current correlations [43].

Green and Kubo showed that the transport coefficients like heat conductivity, shear and the bulk viscosities can be related to the correlation functions of the corresponding flux or the tensor in the thermal equilibrium [18]. The Green-Kubo formalism relates linear transport coefficients to near-equilibrium correlations of dissipative fluxes and treats dissipative fluxes as perturbations to local thermal equilibrium [44]. The relevant formular for Green-Kubo relation for thermal conductivity can be written as [45]

$$\kappa = \frac{V}{3T^2}\int_0^\infty \langle \mathbf{q}_i\left(0\right).\mathbf{q}_i\left(t\right)\rangle\, dt, \tag{5.1}$$

In Eq. (5.1) the brackets <...> stand for the equilibrium average, and no summation is implied over the repeated indices [5, 45] and κ is the thermal conductivity. The time correlation function for the thermal conductivity is also given as [18, 45]

$$\langle \mathbf{q}_i\left(0\right)\mathbf{q}_i\left(0\right)\rangle = \kappa 3T^2\left(\tau_q V\right)^{-1}\exp\left(-t/\tau_q\right), \tag{5.2}$$

The vector $\mathbf{q}_i$ is the Eckart's heat current along the $i = x, y$ and z axis which is defined as

$$\mathbf{q}^i = \frac{1}{V}\sum_{k=1}^{N}\mathbf{p}^i\left(\frac{\mathbf{p}^2}{\mathbf{p}_0^2}\right), \tag{5.3}$$

where by $\mathbf{p}^i$ is the momentum along the $i = x, y$ and z axis and $\mathbf{p}^2 = \mathbf{p}_0^2 - \mathbf{p}_x^2 - \mathbf{p}_y^2 - \mathbf{p}_z^2$ which can be extracted from the UrQMD model output file and τ_q is

the relaxation time of the heat current. If the evolution of the fluctuations of the fluxes is described by the Maxwell-Cattaneo [45], after the integration, Eq. (8) is reduces to

$$\kappa = \tau_q \frac{V}{T^2} \left\langle \mathbf{q}_i \left(0\right) \mathbf{q}_i \left(0\right) \right\rangle . \tag{5.4}$$

We adopt a relativistic microscopic model, namely the UrQMD [6] and perform a molecular-dynamics average for a hadronic gas of mesons in a box to compute the thermal conductivity coefficient of the hadron gas.

Figure 5.1 represents the square expectation of heat current, figure 5.2 represents thermal conductivity, figure 5.3 represents thermal conductivity times temperature and figure 5.4 represents the relaxation time for heat conductivity of a hadron gas as a function of temperature.

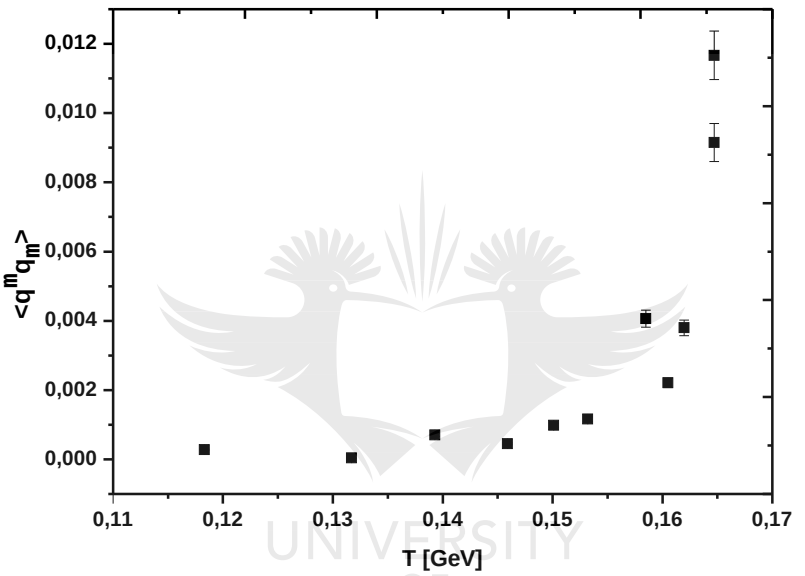

Figure 5.1: The square expectation value of heat current for hadron gas of the pi, the ρ and the K as a function of temperature.

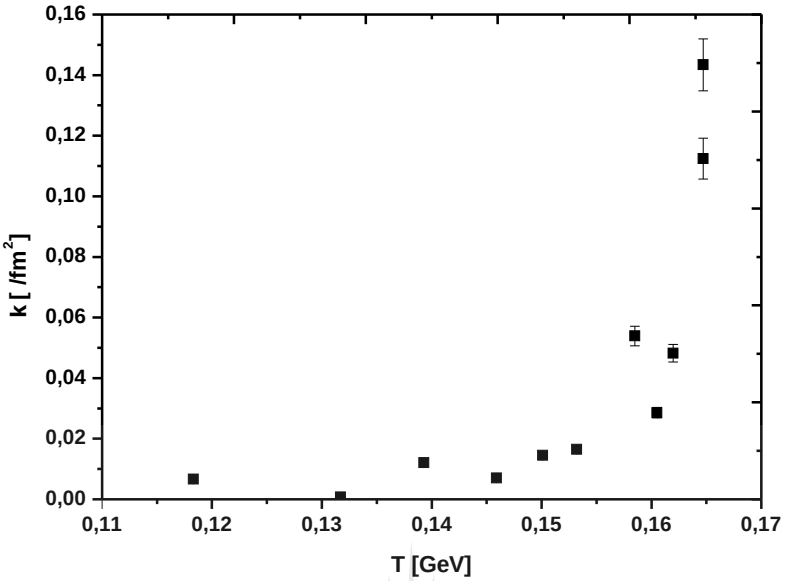

Figure 5.2: The thermal conductivity of a hadron gas of the π, the ρ and the K as a function of temperature.

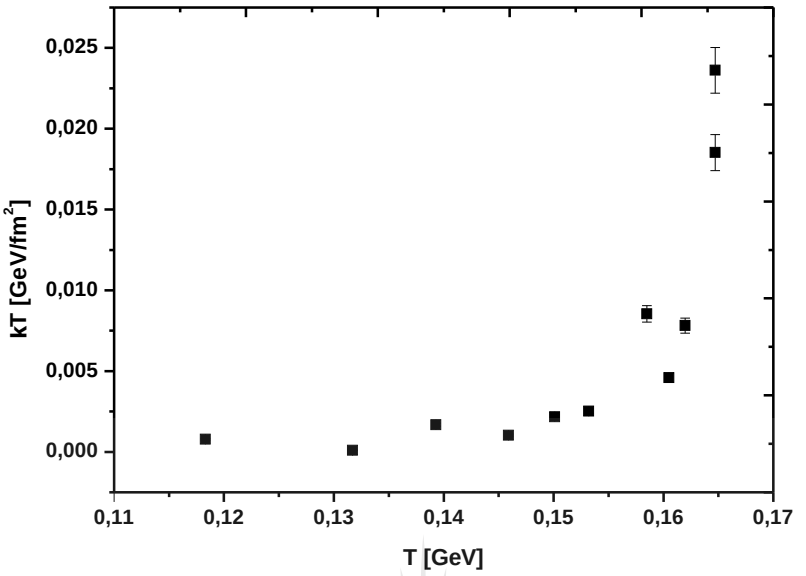

Figure 5.3: The product of thermal conductivity and temperature of a hadron gas of the π, the ρ and the K as a function of temperature.

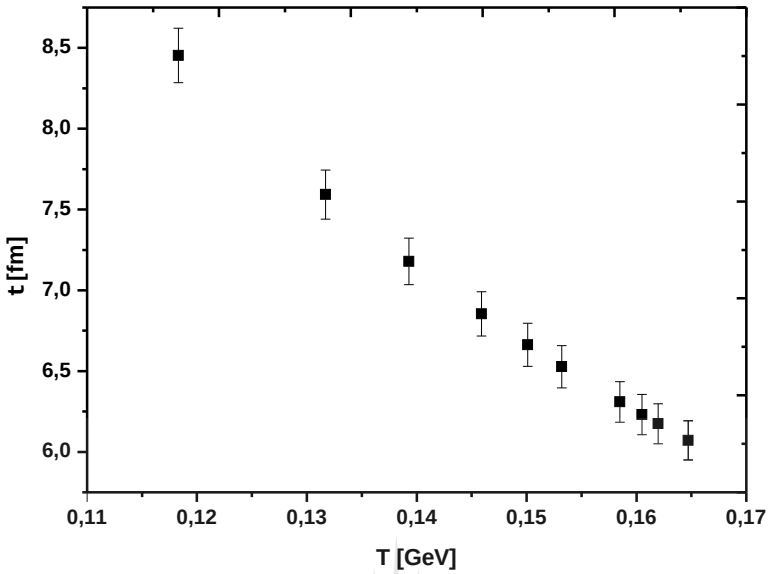

Figure 5.4: The relaxation time for heat conductivity of a hadron gas of the π, the ρ and the K as a function of temperature.

Figure 5.1 shows the square expectation of heat current results obtained from UrQMD model. The heat current increases with increase in temperature. These results are in good comparison with those obtained in [43], where a different model based on an event generator named URASIMA (Ultra-Relativistic AA collision Simulator based on Multiple Scattering Algorithm) was used [46]. The UrQMD square expectation of heat current is much smaller from that obtained in [43], reason might be that for this study we only considered a situation of only meson species and zero baryon number.

Figure 5.2 shows thermal conductivity of hadron gas and figure 5.3 shows the product of thermal conductivity coefficient times temperatureas a function of temperature calculated from UrQMD model. Both, κ, and, κT, increases

with an increase in temperature and the saturation is reached below $T = 0.17$ GeV where the hadronic gas with zero baryon number density is expected to be realized in the central high energy nuclear collisions [5]. The error bars in the graphs are just a statistical errors plotted together with the graphs.

According to our simulation we observed a strong temperature dependence. The temperature behavior of the product of the thermal conductivity and temperature is $\kappa T \sim T^{3.88}$ and for thermal conductvity is $\kappa \sim T^{2.88}$. The temperature dependence of thermal conductivity in this study is greater $T^{3.88} > T^2$ than the one reported by [47] where by the author used Effective Field Theory and it is less $T^{3.88} < T^4$ than the one reported by [43] whereby the author used different simulation model called URASIMA and different system which consist of baryon number density. These differences in temperature dependence might also be due to different masses of the particles involved in each study.

Due to less number of studies done under thermal conductivity coefficient it is difficult to make a proper conclusion from the results obtained, but from the comparison with the little study done already which is related to this topic one can conclude that the results are in good comparison with those reported by [43] and [48] at low temperature and zero baryon number density. At the moment it is not very much clear where the large fluctuation around $T = 160$ MeV comes from in the above figures. Thus a similar study will be done in future which will include the baryon number density and different mesons species at higher energies and large number of events in order to check if one of these factors does play a role for this large fluctuation. For this study the aim was just to test if it is possible to compute thermal conductivity transport coefficient from the UrQMD model using the Green-Kubo relations. The results in this study for

figure 5.2 and figure 5.4 are smaller and that of figure 5.4 are larger than those reported in [43]. The reason might be that the author was using different input parameters for the initialization of the system. In our case we only consider a box of only meson and zero baryon number densities.

Figure 5.4 shows the relaxation time for the heat flux of hot hadron gas as a function of temperature calculated from UrQMD model by fitting the heat correlation functions. The heat relaxation time decreases with an increase in temperature similarly to the one reported in [5, 43].

Chapter 6

Summary and Conclusions

Thermal conductivity transport coefficient of hadron gas was studied using a microscopic transport model the UrQMD to simulate the ultra-relativistic heavy ion collisions in a box with a periodic boundary conditions and V. From the equilibrium state, thermal conductivity was calculated from the heat current - current correlations using the Green-Kubo relations.

In order to study this coefficent a knowledge of hydrodynamic kinetic theory was required and discussed in chapter 2. The relativistic transport model discussed in chapter 3 is of importance in order to understand how was the UrQMD model developed and how does it work in a relativistic way. The microscopic transport model namely the UrQMD was used to simulate ultra-relativistic heavy ion collisions in a box with periodic boundary conditions and volume V was also discussed.

From the saturation of particle number density and convergence of particles slopes to common value of temperatures discussed in chapter 4 it was observed that the system had reached both chemical and thermal equilibrium states. The

Equation of State was studied through the evolution of pressure and energy density with temperature. The results obtained from UrQMD model are in good comparison with the similar studies reported by other authors [3, 5, 6]. From figure 4.7 and 4.8 the power law shows low temperature dependant of meson at low temperatures and high temperature dependant when temperature increases.

It was observed that the square expectation of the heat current, thermal conductivity and the product of thermal conductivity and temperature increase with an increase in temperature. The saturation temperature for square expectation of the heat current, thermal conductivity and the product of thermal conductivity and temperature is below $T = 170$ MeV similarly to that of the equation of state. The power law shows a high temperature dependence for both κ and κT. The heat current relaxation time was calculated from heat correlation function. The relaxation time decrease with an increase in temperature. The results of heat current are in good comparison with those of [43] with regards to the behaviour of the graph.

From the presented results, it can be concluded that it is possible to calculate thermal conductivity transport coefficient using the UrQMD model. More studies are still required for better understanding of the results and the thermal conductivity transport coefficient. The future studies will be to focus on how the thermal conductivity transport coefficient is affected by adding different number of meson species in the box including baryon number density in order to compare with other studies such as that reported by [43, 48], as well as to compare to those who used different model and statistical approach [47, 49].

Appendix A

The input file

In this appendix we discuss the examples of two different input files mentioned in chapter 3 section 3.6. From these two input files, one can initialize how many number of collisions that will be generated, total time of the collisions and time steps required during those collisions. The energy required for collisions can be randomly chosen [34].

In the sample input file for urqmd, one can set the impact parameter and can even initialize the projectile and the target nucleus of their choice needed for collisions [34, 35].

In the infinite matter (box) calculations, one can choose any particles of their choice given in table 3.1 and 3.2 to simulate the collisions. The volume is kept as $10 \times 10 \times 10$ fm^3 [35]. The box calculation is used in this study as the study requires an equilibrium system.

The sample input file for urqmd

```
Pro     197     79
tar     197     79


nev     20
imp     0

elb     11
tim     20      2

eos     0

f13
#f14
f15


xxx
```

Table A.1: An example of the input file used for intialization of the expanding system for nucleas+nucleas collisions.

Table A.1 describes how one can initialize the UrQMD nucleas+nucleas collisions to simulate the ultra-relativistic heavy ion collisions similar to those one performed at CERN, the SPS and the LHC. Table A.2 represent an overview for possible input files flags. Terms in the above table A.1 are defined as follows (# is the explanation of the abbreviation denoted under it) [34, 35].

this is a sample input file for urqmd

projectile nucleas (197: Atomic mass and 79: Atomic number)

pro 197 79

target nucleas (197: Atomic mass and 79: Atomic number)

target 197 79

number of events to calculate (1 stands for one event)

nev 1

time to propagate/calculate (40 fm/c) and output time-interval after at which output is written to files 14 (40 fm/c)

tim 40 40

incident beam energy in AGeV

ene 10.7

impact parameter (nucleus can be intialized to collide either head-on or overlapping)

imp 3.0

equation of state: currently only CASCADE mode

eos 0

f13, f14, f15, f16: suppress output files

no output to files

f15

actual output file we will be using in this studies for extracting UrQMD collision information

#f14

end of file

xxx

label	arguments	description
#	(none)	comment line
xxx	(none)	last line of input–file
pro	Ap Zp	define projectile
PRO	1typ iso3	define special projectile
tar	At Zt	define target
TAR	1typ iso3	define special target
label	arguments	description
nev	nevents	number of events to calculate
tim	tottime outtime	define time of calculation and output
ene	ebeam	incident kinetic beam energy (lab frame)
elb	ebeam	alias for *ene*
plb	pbeam	incident beam momentum (lab frame)
PLB	pmin pmax npbin	incident (min/max) beam momentum for excitation function
PLG	pmin pmax npbin	like *PLB*, log-weighted
ecm	srt	$\sqrt{s}$ for two particle collision
ENE	srtmin srtmax nsrt	incident min/max $\sqrt{s}$ for excitation function
ELG	srtmin srtmax nsrt	like *ENE*, log-weighted
imp	bmax	define impact parameter
IMP	bmin bmax	define impact parameter
eos	EoS	define equation of state
box	dim edens solid para	define box for infinite matter calculation
bpt	1typ iso3 npart pmax	define particle population for box-mode
bpe	1typ iso3 npart	like *bpt*, for given energy density
rsd	seed	seed for random number generator
sub	1typ	keep particle stable
cdt	deltat	Δt between full collision load
f13	(none)	suppress output to unit 13
f14	(none)	suppress output to unit 14
f15	(none)	suppress output to unit 15
f16	(none)	suppress output to unit 16
f19	(none)	suppress output to unit 19
f20	(none)	suppress output to unit 20
cap	index value	set optional parameter in CTParam array
cto	index value	set option in CTOption array

Table A.2: Overview of all the possible input file flags [34].

Infinite matter (box) calculations

```
box dim totenergy solid para
bpt ityp iso3 npart pmax
bpe ityp iso3 npart
```

Table A.3: A sample of an infinite matter (box) calculations [34].

Table A.3 represent the sample of infinite matter (box) calculations. The terms are defined as follows [34, 35].

- dim is the width of (cubic) box (10× 10× 10) fm^3
- totenergy is the total energy content of box in GeV
- solid 1: reflecting walls, 0: periodic boundary conditions
- para 0: standard, 1: use "old" periodic boundary conditions
- ityp is the ID of species (see tables 3.1 and 3.2 for available itypes)
- iso3 2.$Isospin_3$ of species
- npart is the number of particles for species
- pmax is the maximum momentum for fermi-sphere in momentum space [34].

Table A.4 represent a cubic box with periodic boundary conditions used in this study to simulate a pure hadronic state. The data in table A.4 is arranged according to the table A.3.

```
nev     200

tim     400  2
eos      0

box     10 300 0 0
bpe     101  2  80
bpe     104  2  160
bpe     106  1  80

f13
#f14
f15

xxx
```

Table A.4: An example of an input file used for intialization a system of cubic box which impose the periodic boundary conditions.

Appendix B

The output file

The output files allow one to write out a complete history of the collision starting with the initial state, including all the binary collisions and their string decays [34, 35]. Table B.1 represent an example of a sample header of the UrQMD output file produced after simulation. From the first line, the format contains information about the following: first the model name and version, followed by the mass and charge of the projectile and target nucleus, then the reference frame of the calculation, and the incident beam energy as well as the number of test-particles used per nucleon [34, 35].

Table B.2 is an example of the sample body of the UrQMD standard output file produced after simulation. It contains a full history of each event in blocks of data and each block describes interaction [34, 35]. Table B.3 describes the contents of particle vector in the header of collision file.

fromedit.png

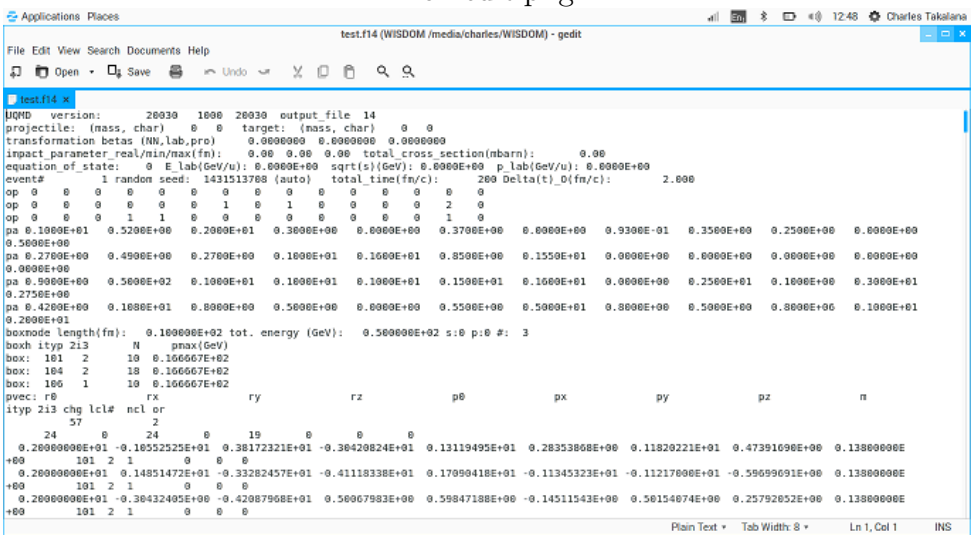

Table B.1: The sample header of the UrQMD output file produced after the simulation.

fromedit21.png

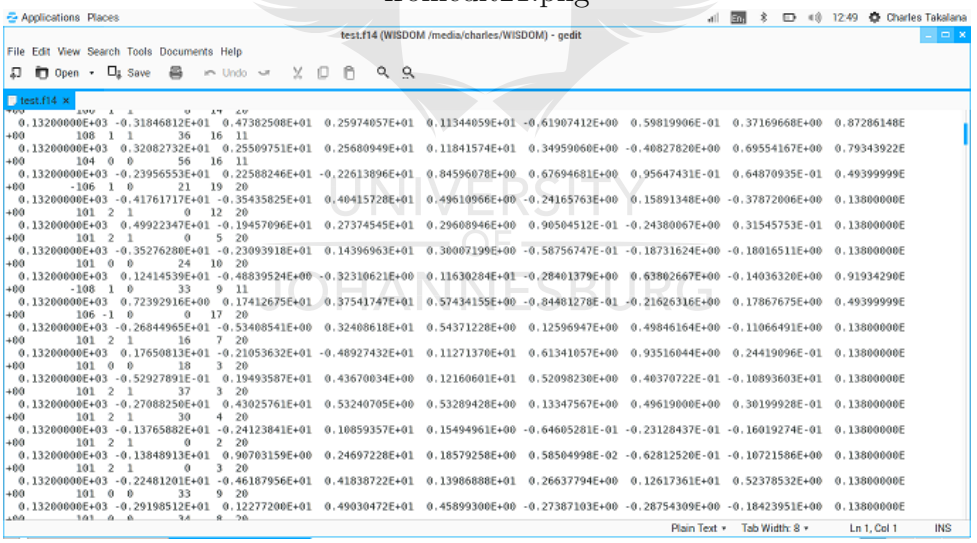

Table B.2: The beginning of sample body of UrQMD standard output file produced after simulation.

column#	contents
1	ind : index of particle
2	t : eigentime of particle in fm/c
3	r_x : x coordinate in fm
4	r_y : y coordinate in fm
5	r_z : z coordinate in fm
6	E : energy of particle in GeV
7	p_x : x momentum component in GeV
8	p_y : y momentum component in GeV
9	p_z : z momentum component in GeV
10	m : mass of particle in GeV
11	$ityp$: particle-ID
12	$2 \cdot I_3$: isospin z-projection (doubled)
13	ch : charge of particle
14	index of last collision partner
15	N_{coll} number of collisions
16	S : strangeness
17	history information (parent process)

Table B.3: Contents of the particle vector in the collision file [34].

Bibliography

[1] Jan Steinheimer, Jörg Aichelin, and Marcus Bleicher. Nonthermal p/π ratio at lhc as a consequence of hadronic final state interactions. *Physical review letters*, 110(4):042501, 2013.

[2] John M Campbell, R Keith Ellis, and Ciaran Williams. Vector boson pair production at the lhc. *Journal of High Energy Physics*, 2011(7):1–36, 2011.

[3] EL Bratkovskaya, W Cassing, C Greiner, M Effenberger, U Mosel, and A Sibirtsev. Aspects of thermal and chemical equilibration of hadronic matter. *Nuclear Physics A*, 675(3):661–691, 2000.

[4] Nasser Demir and Anton Wiranata. Hadronic shear viscosity: A comparison between the green-kubo and chapmann enskog methods. In *Journal of Physics: Conference Series*, volume 535, page 012018. IOP Publishing, 2014.

[5] Azwinndini Muronga. Shear viscosity coefficient from microscopic models. *Physical Review C*, 69(4):044901, 2004.

[6] Steffen A Bass, Mohamed Belkacem, Marcus Bleicher, Mathias Brandstetter, L Bravina, Christoph Ernst, Lars Gerland, M Hofmann, S Hofmann,

Jens Konopka, et al. Microscopic models for ultrarelativistic heavy ion collisions. *Progress in Particle and Nuclear Physics*, 41:255–369, 1998.

[7] MI Gorenstein, M Hauer, and ON Moroz. Viscosity in the excluded volume hadron gas model. *Physical Review C*, 77(2):024911, 2008.

[8] Michael Mitrovski, Tim Schuster, Gunnar Gräf, Hannah Petersen, and Marcus Bleicher. Charged-particle (pseudo-)rapidity distributions in $p + \overline{p}/p+p$ and Pb+Pb/Au+Au collisions from urqmd calculations at energies available at the cern super proton synchrotron to the large hadron collider. *Phys. Rev. C*, 79:044901, Apr 2009.

[9] Francesco Becattini, Marcus Bleicher, Thorsten Kollegger, Tim Schuster, Jan Steinheimer, and Reinhard Stock. Hadron formation in relativistic nuclear collisions and the qcd phase diagram. *Physical review letters*, 111(8):082302, 2013.

[10] Marcus Bleicher, Stephan Endres, Jan Steinheimer, and Hendrik van Hees. Recent results from the urqmd hybrid model for heavy ion collisions. *arXiv preprint arXiv:1503.07371*, 2015.

[11] Qingfeng Li, Jan Steinheimer, Hannah Petersen, Marcus Bleicher, and Horst Stöcker. Effects of a phase transition on hbt correlations in an integrated boltzmann+ hydrodynamics approach. *Physics Letters B*, 674(2):111–116, 2009.

[12] Chungsik Song and Volker Koch. Chemical relaxation time of pions in hot hadronic matter. *Physical Review C*, 55(6):3026, 1997.

[13] LV Bravina, M Brandstetter, EE Zabrodin, M Bleicher, H Stöcker, W Greiner, S Soff, and SA Bass. Local equilibrium in heavy-ion collisions. *Phys. Rev. C*, 62(nucl-th/0011011):064906, 2000.

[14] Mohamed Belkacem, Mathias Brandstetter, Steffen A Bass, Marcus Bleicher, L Bravina, Mark I Gorenstein, Jens Konopka, Ludwig Neise, Christian Spieles, Sven Soff, et al. Equation of state, spectra, and composition of hot and dense infinite hadronic matter in a microscopic transport model. *Physical Review C*, 58(3):1727, 1998.

[15] D Fernandez-Fraile and A Gomez Nicola. Transport coefficients and resonances for a meson gas in chiral perturbation theory. *The European Physical Journal C-Particles and Fields*, 62(1):37–54, 2009.

[16] M Greif, F Reining, I Bouras, GS Denicol, Z Xu, and C Greiner. Investigation of heat conductivity in relativistic systems using a partonic cascade. *arXiv preprint arXiv:1301.1190*, 2013.

[17] Savas Berber, Young-Kyun Kwon, and David Tománek. Unusually high thermal conductivity of carbon nanotubes. *Physical review letters*, 84(20):4613, 2000.

[18] C Wesp, A El, F Reining, Z Xu, I Bouras, and C Greiner. Calculation of shear viscosity using green-kubo relations within a parton cascade. *Physical Review C*, 84(5):054911, 2011.

[19] S Plumari, A Puglisi, F Scardina, and V Greco. Shear viscosity of a strongly interacting system: Green-kubo vs. chapman-enskog and relaxation time approximation. *arXiv preprint arXiv:1208.0481*, 2012.

[20] Particle Data Group et al. *Particle physics booklet*. in the Americas, Australasia, or the Far East, write to: Particle Data Group, Lawrence Berkeley National Laboratory, 2004.

[21] Masahiro Ibe, Hitoshi Murayama, and TT Yanagida. Breit-wigner enhancement of dark matter annihilation. *Physical Review D*, 79(9):095009, 2009.

[22] Rudolf Baier, Paul Romatschke, Dam Thanh Son, Andrei O Starinets, and Mikhail A Stephanov. Relativistic viscous hydrodynamics, conformal invariance, and holography. *Journal of High Energy Physics*, 2008(04):100, 2008.

[23] László P Csernai. *Introduction to relativistic heavy ion collisions*. Wiley New York, 1994.

[24] Sangyong Jeon and Laurence G Yaffe. From quantum field theory to hydrodynamics: Transport coefficients and effective kinetic theory. *Physical Review D*, 53(10):5799, 1996.

[25] S.R. de Groot, W.A. van Leeuwen, and Ch.G. van Weert. *Relativistic Kinetic Theory*. North-Holland Publishing Company Amsterdam.New York.Oxford, 1980.

[26] Paul Romatschke. New developments in relativistic viscous hydrodynamics. *International Journal of Modern Physics E*, 19(01):1–53, 2010.

[27] I Bouras, E Molnar, H Niemi, Z Xu, A El, O Fochler, C Greiner, and DH Rischke. Investigation of shock waves in the relativistic riemann prob-

lem: A comparison of viscous fluid dynamics to kinetic theory. *Physical Review C*, 82(2):024910, 2010.

[28] Ulrich Heinz, Huichao Song, and Asis K Chaudhuri. Dissipative hydrodynamics for viscous relativistic fluids. *Physical Review C*, 73(3):034904, 2006.

[29] Marcus Bleicher, E Zabrodin, Christian Spieles, Steffen A Bass, Christoph Ernst, Sven Soff, L Bravina, Mohamed Belkacem, H Weber, Horst Stöcker, et al. Relativistic hadron-hadron collisions in the ultra-relativistic quantum molecular dynamics model. *Journal of Physics G: Nuclear and Particle Physics*, 25(9):1859, 1999.

[30] PANDA collaboration et al. Strong interaction studies with antiprotons. *Technical Progress Report, GSI, Darmstadt*, 2005.

[31] Miklos Gyulassy. For rhic.

[32] Thomas Lang, Hendrik van Hees, Jan Steinheimer, and Marcus Bleicher. Heavy quark transport in heavy ion collisions at rhic and lhc within the urqmd transport model. *arXiv preprint arXiv:1211.6912*, 2012.

[33] Christian Spieles, Ramona Vogt, Lars Gerland, Steffen A Bass, Marcus Bleicher, Horst Stöcker, and Walter Greiner. Modeling j/ψ production and absorption in a microscopic nonequilibrium approach. *Physical Review C*, 60(5):054901, 1999.

[34] UrQMD Collaboration et al. The urqmd user guide (2014).

[35] SA Bass, M Belkacem, M Bleicher, M Brandstetter, L Bravina, C Ernst, L Gerland, M Hofmann, S Hofmann, J Konopka, et al. The ultra relativistic quantum molecular dynamics (urqmd) model is a transport model for simu-lating heavy ion collisions in the energy range from sis to rhic. it runs on various unix-based com-puting platforms. current implementations include ibm/aix (xlf), gnu/linux (g77, ifc), sgi/irix, dec-unix and sun/solaris. urqmdis designed as multipurpose tool for studying a wide variety of heavy ion related effects rang. *J. Phys*, 25:1859–1896, 1999.

[36] Larissa V Bravina, Eugene E Zabrodin, Mark I Gorenstein, Steffen A Bass, Mohamed Belkacem, Marcus Bleicher, Mathias Brandstetter, Christoph Ernst, Markus Hofmann, Ludwig Neise, et al. Local equilibrium in heavy ion collisions: Microscopic model versus statistical model analysis. *Physical Review C*, 60(2):024904, 1999.

[37] Nobuo Sasaki. A study of the thermodynamic properties of a hot, dense hadron gas using an event generator hadro-molecular-dynamical calculation. *Progress of theoretical Physics*, 106(4):783–805, 2001.

[38] Azwinndini Muronga. Relativistic dynamics of non-ideal fluids: Viscous and heat-conducting fluids. ii. transport properties and microscopic description of relativistic nuclear matter. *Physical Review C*, 76(1):014910, 2007.

[39] W Reisdorf and HG Ritter. Collective flow in heavy-ion collisions. *Annual Review of Nuclear and Particle Science*, 47(1):663–709, 1997.

[40] Marcus Bleicher, Manuel Reiter, Adrian Dumitru, Jörg Brachmann, Christian Spieles, Steffen A Bass, Horst Stöcker, and Walter Greiner. Dis-

tinguishing hadronic cascades from hydrodynamic models in pb (160 a gev)+ pb reactions by impact parameter variation. *Physical Review C*, 59(4):R1844, 1999.

[41] Subrata Pal. Shear viscosity to entropy density ratio of a relativistic hagedorn resonance gas. *Physics Letters B*, 684(4):211–215, 2010.

[42] Lydéric Bocquet and Jean-Louis Barrat. Hydrodynamic boundary conditions, correlation functions, and kubo relations for confined fluids. *Physical review E*, 49(4):3079, 1994.

[43] Shin Muroya. Transport coefficients of relativistic causal hydrodynamics for hadrons. *arXiv preprint hep-ph/0702220*, 2007.

[44] Nasser Demir and Steffen A Bass. Extracting hadronic viscosity from microscopic transport models. *The European Physical Journal C*, 62(1):63–68, 2009.

[45] Azwinndini Muronga. Generalized entropy and transport coefficients of hadronic matter. *The European Physical Journal-Special Topics*, 155(1):107–113, 2008.

[46] Shin Muroya and Nobuo Sasaki. A calculation of the viscosity to entropy ratio of a hadronic gas. *Progress of theoretical physics*, 113(2):457–462, 2005.

[47] Juan M Torres-Rincon. Hadronic transport coefficients from effective field theories. *arXiv preprint arXiv:1205.0782*, 2012.

[48] Romulo Rougemont, Jorge Noronha, and Jacquelyn Noronha-Hostler. Suppression of baryon diffusion and transport in a baryon rich strongly coupled quark-gluon plasma. *Physical Review Letters*, 115(20):202301, 2015.

[49] M Greif, F Reining, I Bouras, GS Denicol, Z Xu, and C Greiner. Heat conductivity in relativistic systems investigated using a partonic cascade. *Physical Review E*, 87(3):033019, 2013.